

Does the Laxmi Ridge continue towards the Laccadive Ridge? New insights from an integrated geophysical study.

Akhil Mishra^{a,b#}, Anil KumarChaubey^{a,b*}, Shравan Kumar^{a,c}, Pitchika Vinay Kumar^{a,\$}, Pankaj Kumar^{a,b}, Kanchan ManiDubey^{a,d}

^a CSIR-National Institute of Oceanography, Regional Centre, Lokhandwala Road, Andheri (West), Mumbai-400053, India.

^b Academy of Scientific and Innovative Research, CSIR-National Institute of Oceanography, Goa, India.

^cDepartment of Geophysics, Institute of Science, Banaras Hindu University, Varanasi- 221005, India

^dDepartment of Marine Sciences, Goa University, Taleigao Plateau, Goa-403206, India

[#] Present address: CSIR-National Geophysical Research Institute, Hyderabad, India

^{\$} Present address: Centre for Earth, Ocean and Atmospheric Sciences, University of Hyderabad, Hyderabad

*Corresponding author: chaubey@nio.org

Abstract

The Laxmi and Laccadive ridges are two major aseismic ridges in the NW Indian Ocean. Bathymetry, gravity and magnetic data and their derivatives are analyzed and modelled to assess the interrelationship between both the ridges as well as to establish their crustal structure, nature and isostatic compensation. Boundaries of the Laxmi and Laccadive ridges are delineated by tilt derivative with constraints from available seismic-sections. Integrated gravity and magnetic models reveal that both the ridges have almost similar crustal layers and are underplated all along its length. Crustal models also depict that both the ridges are carpeted with flood basalt and heavily intruded. 3D coherence between Mantle Bouguer Anomaly and residual bathymetry reveals that the elastic plate thickness and subsurface to surface load ratio for both the ridges vary from 3 to 4 km and 0.7 to 0.8, respectively. Several characteristic similarities viz. crustal structure and nature, elastic plate thickness, magmatism have been observed for both the ridges. Seismic sections near the junction of the ridges suggest that the basement high corresponding to the Laxmi Ridge is further continued towards the Laccadive Ridge. In addition, the northwestern part of the Laccadive Ridge has NW-SE structural lineaments similar to that of the NW-SE segment of the Laxmi Ridge. Based on results of the present and previous studies, we infer that (i) the Laxmi Ridge is extended southeastward towards the Laccadive Ridge, (ii) both the ridges are continental slivers which are underplated as well as intruded and carpeted by volcanics, and (iii) both the ridges are locally compensated.

Keywords: Laxmi Ridge; Laccadive Ridge; NW Indian Ocean; Gravity and Magnetic Data; Tilt Derivative; 3D Coherence.

1. Introduction

The Laxmi and Laccadive ridges (Fig. 1) are two most prominent physiographic and aseismic ridges in the NW Indian Ocean. The Laxmi Ridge runs in the NW-SE direction between 14.5°N and 19.3°N and then westward with E-W strike from 19.3°N, 65.8°E (Fig. 1). The average water depth and maximum relief over the ridge are ~3.5 km and ~1.2 km, respectively (Mishra et al., 2018). The estimated maximum depth to Moho under the Laxmi Ridge is around 21-23 km (Naini and Talwani, 1983; Minshull et al., 2008; Misra et al., 2015) which implies that the ridge crust is thicker than typical oceanic crust and thinner than continental crust. Both free-air and isostatic gravity anomalies are low over it, whereas magnetic anomaly is irregular, implying non-seafloor spreading type magnetic anomaly. Crustal nature of the Laxmi Ridge is considered as continental by most of the researchers (Naini and Talwani, 1983; Bhattacharya et al., 1994; Talwani and Reif, 1998; Todal and Edholm, 1998; Radhakrishna et al., 2002; Krishna et al., 2006; Ajay et al., 2010; Arora et al., 2012; Bhattacharya and Yatheesh, 2015; Nair et al., 2015; Mishra et al., 2018); however, few studies favour oceanic origin of the ridge (Pandey et al., 1995; Singh, 1999; Misra et al., 2015).

The Laccadive Ridge (Fig. 1) is the northern segment of aseismic Chagos-Laccadive Ridge and lies approximately north of 10°N. About 20 islands and banks are scattered over the ridge (Bhattacharya and Chaubey, 2001). Free-air anomaly over the ridge is negative and subdued; however, relatively positive anomaly is observed above the crestal region. The magnetic signature is subdued over the eastern flank of the Laccadive Ridge, whereas the western flank is associated with several prominent high amplitude anomalies. Seismic refraction results reveal that the Moho lies at depth of 18-19 km implying that the crust beneath the ridge is thicker than normal oceanic crust and thinner than continental crust (Naini and Talwani, 1983; Bhattacharya and Chaubey, 2001). Regarding the origin of the Laccadive Ridge, a number of hypotheses exist in the literature. It has been considered as a transition zone between oceanic crust in the west and continental crust in the east (Narain et al., 1968), leaky transform fault (Fisher et al., 1971; McKenzie and Sclater, 1971; Avraham and Bunce, 1977), the Réunion hotspot trace (Whitmarsh, 1974; Duncan, 1981; Shipboard Scientific Party, 1988; Richards et al., 1989; Duncan, 1990), a continental fragment (Naini and Talwani, 1983; Murty et al., 1999; Bhattacharya and Yatheesh, 2015), continental fragment intermingled with volcanic intrusives (Chaubey et al., 1998, 2002a, 2008) and at some places it might be originated by magmatism emplaced over an oceanic crust (Chaubey et al., 1995).

There is also a lack of understanding regarding interrelationship of both the ridges. Naini and Talwani (1983) proposed that morphologically, the Laxmi Ridge is NW continuation of the Laccadive Ridge, while Talwani and Reif (1998) suggested that the Laccadive Ridge is continued

towards the north, not towards the Laxmi Ridge. Todal and Edholm (1998) believed that the Laxmi Ridge is a separate feature from the Laccadive Ridge based on crustal density models. These studies warrant an integrated geophysical approach to establish their interrelationship. Seismic, bathymetry, gravity and magnetic data over the Laxmi and Laccadive ridges are analysed and modelled in the present study to (i) determine crustal structure and nature of the ridges (ii) delineate boundaries and structural features of the ridges (iii) relook into the isostatic compensation mechanism and subsurface loading along the ridges, and (iv) decipher interrelationship between both the ridges.

2. Geophysical Data

Ship-borne bathymetry, gravity and magnetic data used in the present study were acquired during different cruises of ORV Sagar Kanya (SK12, SK 22, SK50, SK64, SK79, and SK162), RV Sindhu Sankalp (SSK36, SSK52, and SSK96) and DSV Nand Rachit (NR05) during 1984-2016. The surveyed tracks are shown in Figure 2. From all the profiles, spikes and other erroneous data were removed. Total magnetic field intensity data have been reduced to residual magnetic anomalies by subtracting the International Geomagnetic Reference Field of the appropriate epoch. Free-Air gravity Anomalies (FAA) data were obtained by applying normal and Eötvös corrections to the measured gravity data. Bathymetry, magnetic and gravity data were first smoothed using 5 km Gaussian filter and then resampled at 0.4 km interval for crustal structure modelling across both the ridges.

'Bedrock' version of ETOPO1, one arc-minute global relief model (Amante and Eakins, 2009) for bathymetry grid data, has also been utilised. Free-air anomaly data are obtained from global marine gravity data (grav.img.24.1) of Sandwell et al. (2014). Sediment thickness model utilised in this work is taken from Divins (2003). The geoid grid for the present study area was extracted from geoid data generated for the northern Indian Ocean by Sreejith et al. (2013). Average P-wave velocity for each crustal layers has been estimated using refraction data of the Western and Eastern basins (Naini and Talwani, 1983) covering the study area (Fig. 1). These average velocities are converted into density using Brocher (2005) formula (Table-1) for forward gravity modelling.

Published seismic sections for delineation of boundaries of the ridges and basement constraints in integrated gravity-magnetic crustal modelling are taken from Ajay (2011), Krishna et al. (2006) and Misra et al. (2015) (Fig. 2). Single-channel seismic data from the National Centers for Environmental Information (NCEI), formerly known as National Geophysical Data Centre (NGDC), are also utilized. The single-channel seismic data from cruises RV Vema (1977), RV Robert D. Conrad (1974) falling within the study area are compiled and utilized in this study.

3. Theory and method

3.1. Tilt derivative of free-air anomaly

Tilt derivative is one of the best tools for locating the edge of the source. It is defined as the ratio of the first vertical derivative of the potential field (f) to the horizontal gradient of the field (Miller and Singh, 1994).

$$\begin{aligned} \text{Tilt angle} &= \tan^{-1} \frac{\text{vertical component of gradient}}{\text{horizontal component of gradient}} \\ &= \tan^{-1} \frac{\partial f / \partial z}{\sqrt{(\partial f / \partial x)^2 + (\partial f / \partial y)^2}} \dots\dots\dots (1) \end{aligned}$$

3.2. Coherence analysis

The theoretical coherence between Mantle Bouguer Anomaly (MBA) and residual bathymetry is computed from the following equations (Forsyth, 1985; Luis and Neves, 2006):

$$\gamma^2(k) = \frac{(1+(F/\xi)^2\phi)^2}{(1+(F/\xi)^2)(1+F^2\phi^2)}, \dots\dots\dots (2)$$

where,
$$\phi = 1 + \frac{D(2\pi k)^4}{(\rho_c - \rho_w)g}, \xi = 1 + \frac{D(2\pi k)^4}{\Delta\rho g}, D = \frac{ET_e^3}{12(1-\sigma^2)}$$

and $\Delta\rho = \rho_m - \rho_c$

Where, D is flexural rigidity and T_e is elastic plate thickness. Other notations and their values are presented in Table-2. The observed coherence is computed by the following relation:

$$\gamma^2(k) = \frac{C(k)C^*(k)}{E_g(k)E_b(k)} \dots\dots\dots (3)$$

Where C(k) is the cross-spectrum of bathymetry and gravity; the asterisk (*) denotes the complex conjugate; $E_g(k)$ and $E_b(k)$ are the power spectrums of gravity and bathymetry, respectively.

MBA data of the study area are generated by subtracting gravity effect of seafloor relief, sediments and crust-mantle interface from free-air gravity anomaly assuming an average crustal thickness of 6 km. Sediment thickness is multiplied by a correction factor 0.48 (Crough, 1983) to remove its isostatic effect and then subtracted from the bathymetry to get residual bathymetry. Computation of gravity anomaly from bathymetry and density contrast is carried out using an algorithm developed by Parker (1972).

3.3. Integrated gravity and magnetic modelling

2D integrated gravity and magnetic forward modelling has been carried out using GM-SYS module of Oasis Montaj software. The computational scheme is based on the method of Talwani et al. (1959) and makes use of algorithms illustrated in Won and Bevis (1987). To eliminate the edge effect, all the models are extended to ± 30000 km (infinity) in both the side of the X direction. In forward

gravity and magnetic modelling, initially, a priori geological model, well constrained by other geophysical proxies is created and its gravity and magnetic responses are calculated to compare with observed gravity and magnetic value. If there is a good match between observed and calculated values then the geological model is the final crustal model, if not, then in an interactive way, the model is kept on modifying till the best match is obtained.

As a first step, an initial crustal model is prepared along a selected transect by integrating bathymetry, seismic reflection and refraction data available along the transect or close to the transect. Main crustal layers are constructed based on P-wave velocities obtained from refraction data. The average velocity of each layer is calculated and density of the layer is computed using the velocity-density formula of Brocher (2005).

Magnetic parameters for computation of magnetic response of crustal layers are taken from published results of nearby area (Krishna et al., 2006; Rao et al., 2010). Forward gravity and magnetic modelling was performed by continuously applying small adjustments to the geometries of crustal layers to obtain a crustal model which satisfies both the geometrical constraints and an acceptable fit between observed and calculated gravity and magnetic anomalies.

3.4. 3D Euler deconvolution and depth estimation

3D Euler deconvolution method is utilized for determining depth and location of magnetic source from gridded magnetic data. The Euler deconvolution is a widely used technique and is based on solving Euler's homogeneity equation

$$(x - x_0) \frac{\partial F}{\partial x} + (y - y_0) \frac{\partial F}{\partial y} + (z - z_0) \frac{\partial F}{\partial z} = -NF \dots\dots\dots(4)$$

Where, F is the total magnetic field anomaly observed at (x, y, z) due to magnetic source located at (x₀, y₀, z₀) and N is the Structural Index (SI). The advantage of this method is that the magnetic data need not be reduced to pole, so that remanence is not an interfering factor (Reid et al., 1990). Since the structural index is dependent on source geometry, and observed anomaly might have different sources, therefore, the above equation should be solved for a number of indices. The indices, which give good clusters of Euler solutions, are considered for interpretation. In the present study, Euler deconvolution is utilised for determining the location of the faults, i.e. for SI=0.

4. Analyses and results

4.1. Boundaries of the Laxmi and Laccadive ridges

Boundaries of the Laxmi and Laccadive ridges are delineated based on three constraints, (i) tilt angle of the FAA, (ii) available seismic reflection profiles across the ridges, and (iii) crustal models generated from integrated modelling of gravity and magnetic data. The tilt angle of FAA in the study

area has been calculated utilising the equation (1) and presented in Figure 3. The tilt angle clearly depicts edges of structural features present in the study area. The edges of the features such as the Laxmi, Laccadive ridges, Raman, Panikkar, seamounts, Wadia Guyot, shelf break, slope are much clearer than that depicted in the FAA map.

Tilt angle has the attractive property of being positive over the source, crosses the zero line of tilt angle at or near the edge of source body and negative outside the region (Miller and Singh, 1994). Boundary of the Laxmi Ridge is delineated by following the zero contour line smoothly (Fig. 3). The boundary of the Laxmi Ridge is further constrained by the seismic sections (RE01, RE02, RE11, RC1707_59, RC1707_63, RC1707_64, V3408_3, V3407_9 and V3407_10) and crustal models generated through integrated gravity and magnetic modelling across the ridge. The final boundary is shown in Figure 3. The Laxmi Ridge runs in the NW-SE direction between 14.5°N and 19.3°N and then westward with an E-W strike from 19.3°N, 65.8°E. NW-SE part is wider than the E-W part of the ridge. Width of the E-W part varies from 25 to 60 km with an average width of ~40 km. Width of NW-SE part increases towards SE from ~70 km to 135 km. There is a sudden disruption of the boundary between 15.2°N and 15.8°N and width decreases from 120 km to 70 km and then further increases southeastward. The NW-SE part of the Laxmi Ridge between 15°N and 17°N reveals several NW-SE trending features which are limited within its boundary. In addition, there are other several localized isolated features randomly distributed over the ridge.

Boundary of the Laccadive Ridge is also delineated by following the zero contour line smoothly. This boundary is further constrained by the boundaries determined from seismic sections (SK12-08, SK12-07, SK12-06, SK12-03, RE13, RE15, RE17, RE19, and RE23) across the ridge. The final boundary of Laccadive Ridge is shown in Figure 3. The Laccadive Ridge is stretched from 7.3°N to 15°N and parallel to subparallel to the shelf break off southwestern India. It abuts against oceanic crust of Western Basin on its western side and the Laccadive Basin on its eastern side. Its width is almost same (~280 km) between 9.5°N and 15°N. South of 9.5°N, the width reduces ~220 km to ~100 km. NE-SW to N-S and NW-SE structural trends are well evident in the tilt angle map which are restricted to the boundary of the Laccadive Ridge. From these trends, it is also clear that western flank of the Laccadive Ridge, between 10°N and 14.5°N, exhibits structural NW-SE trends which are different to that of the eastern flank displaying N-S to NE-SW trends.

4.2. Magnetic characteristics and fault lineaments

Ship-borne magnetic data along all the tracks (Fig. 2) are further analyzed for crossover error as the data have been compiled from the different cruises. The crossover errors at each intersection are estimated and appropriate linear models of systematic corrections for each track are determined

using the 'x2sys' package of Wessel (2010). The crossover corrected data is gridded with minimum curvature method and the resultant magnetic grid is utilized to generate magnetic anomaly map of the study area (Fig. 4) for further analysis and interpretation.

Magnetic anomaly over the Laxmi Ridge (Fig. 4) ranges from -364 nT (minimum) to 431 nT (maximum). It is noticeable that a major part of the Laxmi Ridge is associated with magnetic anomaly lows with a few magnetic highs at locations. The northernmost part of the ridge exhibits prominent magnetic anomaly lows trending in EW direction. An EW trending magnetic high near 18.5°N, 66°E, located at the junction between E-W and NW-SE segments of the ridge, seems to act as a boundary between these two segments. A linear magnetic high trending NE-SW is located at ~17°N. At the southern part of the ridge, where the boundary is disrupted, WNW-ESE trending prominent magnetic low and high are present. Towards the Western Basin side, the Laxmi Ridge terminates against magnetic anomaly Chron 28n. Magnetic anomaly over the Laccadive Ridge ranges from -475 nT to 400nT and the ridge is characterized by several magnetic anomalies lows and highs. Distribution of magnetic highs is predominant as compared to magnetic lows. There are few distinct zones over the ridge where amplitudes (peak to trough) of magnetic anomalies are extremely high.

3D Euler deconvolution is applied on gridded magnetic data with a window size of 30 km × 30 km. Since $SI = 0$ gives solution for faults, the Euler solutions are obtained for $SI = 0$ to identify and locate faults on both the ridges. The solutions are plotted on the magnetic anomaly map and presented in Figure 4(a). As the present study focuses on the Laxmi and Laccadive ridges, the Euler solutions outside the boundaries of the ridges are not considered. Euler solutions depict that there are several solutions corresponding to faults/contacts over the ridges.

The Laxmi Ridge between 62.6°E and 66.5°E is associated with prominent clusters of the Euler solutions which trend E-W and lie adjacent to the boundary of the ridge (Fig. 4). These solutions correspond to contacts between Laxmi Ridge and oceanic crust of either side. Further, where Laxmi Ridge changes its trend from E-W to NW-SE, there is magnetic high zone which is associated with Euler solution trending E-W and ENE-WSW. Interpretation suggests that it is a fault zone which separates the Laxmi Ridge into two aforesaid part of the ridge. At the transition of the Laxmi Ridge and the Laxmi Basin, there is no cluster of Euler Solutions; whereas western side, i.e. junction of Western Basin and Laxmi Ridge there are several NW-SE trending linear clusters. At the southern part of the Laxmi Ridge where the boundary of the ridge is disrupted, Euler solutions also display a good cluster trending NW-SE which separates prominent magnetic low from magnetic high (Fig. 4).

On the basis of disrupted boundary and Euler solution, it is interpreted that southernmost part of the Laxmi Ridge might have tried to split from the remaining part of the ridge. The southern end of the Laxmi Ridge is associated with prominent NW-SE trending faults/contacts. This fault seems to further continue towards the northern part of the Laccadive Ridge (Fig. 4).

In comparison to the Laxmi Ridge, there are many linear clusters of Euler solutions over the Laccadive Ridge (Fig. 4). Interpreted Euler solutions at the southern end of the Laxmi Ridge is further continued southeastward and parallel to the adjacent northern boundary of the Laccadive Ridge. The northern boundary of the eastern flank of the Laccadive Ridge is abutted by a prominent ENE-WSW trending fault/contact. The western boundary of the Laccadive Ridge is associated with several NNW-SSE Euler solutions of limited extent (Fig. 4). These lineations/faults, in general, are parallel to subparallel to the adjacent boundary of the Laccadive Ridge. The eastern boundary of the Laccadive Ridge is also associated with several N-S, NE-SW, E-W trending Euler solutions. From the map (Fig. 4b) it is noticed that eastern flank of the ridge exhibit more clusters of Euler solutions than the western flank. Trends of major Euler solutions are N-S, NW-SE, NNW-SSE, NE-SW, ENE-WSW, E-W. There are several horst graben structures reported over the ridge, and therefore it is interpreted that these solutions correspond to the basement faults.

4.3. Coherence, elastic plate thickness and subsurface loading

Coherence between MBA and residual bathymetry is computed using Eq. 3 for the region encompassing the Laccadive Ridge. The computed coherence as a function of wavelength is shown in Figure 5(a). The coherence reaches to unity for the long wavelength (>400 km), which is an indication of locally compensated topography, suggesting that bathymetry is not supported by flexural strength of the lithosphere. The coherence for the wavelength less than 50 km displays noise influenced values; therefore, these values are not incorporated in the analysis. The wavelength of the transition zone from low coherence to high coherence provides an indication of flexural rigidity of the lithosphere and in this zone (50 km to 400 km), observed coherence values rise sharply from 0.3 to 0.97.

The theoretical coherence between MBA and residual bathymetry is computed as a function of wavelength from Eq. 1, for a range of loading ratio (F) and T_e values (Fig. 5a). Theoretical coherence, for $T_e=2, 3, 5$ and 7 km and for a fixed value of $F=0.7$, are plotted (Fig. 5a, blue coloured curve) on a semi-logarithmic graph together with observed coherence (Fig. 5a, stars with error-bars in red colour) for comparison. The values of observed coherence are falling between the theoretical

coherence curves computed with $T_e=2$ km and 7 km. The narrow width of the transition zone (50-300 km) is suggestive of similar T_e trend along the Laccadive Ridge.

For constraining the values of T_e and load ratio F , Root Mean Square (RMS) error between observed and theoretical coherence is examined. The value of T_e and F are systematically varied from 0.0001 km to 20 km and from 0 to 5 respectively to compute the RMS error. For each combination of T_e and F , the RMS error between theoretical and observed coherence is calculated and plotted against T_e and F (Fig. 5b). The result shows that the RMS error is minimum for $T_e=3$ km and $F=0.7$, which is shown by a star in Figure 5(b). This implies that the amplitude of subsurface load at Moho contributes 70% to that of the surface load. The coherence curve for the best match ($T_e=3.0$ km and $F=0.7$.) is shown with green colour in Figure 5(a). Mishra et al. (2018) estimated value of T_e and F over the Laxmi Ridge in a similar way. The results indicate that the T_e is 3-4 km and F is 0.8 for the Laxmi Ridge. Therefore, it is interpreted that the elastic plate thickness of the ridges are low and the lithospheric plate is weak.

4.4. Geoid to topography ratio over the Laccadive Ridge

It is well known that the longer wavelength (>4000 km) geoid and topographic anomalies are due to density anomalies in the lower mantle (Bowin, 1983) and cooling of the lithosphere (Haxby and Turcotte, 1978), while shorter wavelength (<330 km) contain signal from lithosphere flexure and variation in crustal thickness. However, geoid is linearly related to the topography between wavelengths 330 and 4000 km (Sandwell & Renkin, 1988); therefore, the Geoid to Topography Ratio (GTR) analysis of this waveband can be used to understand isostatic compensation mechanism of oceanic features (Haxby and Turcotte, 1978; Sandwell and Mackenzie, 1989).

Filtered residual geoid and topography of the entire western Indian Ocean are generated by passing gridded geoid height and sediment corrected bathymetry data sets in the waveband 330-4000 km. In general, the Laccadive Ridge is associated with negative residual geoid and its values ranges from -4.6 m to -2.8 m (Fig. 6a). Residual topography varies from -1.1 km to 1.6 km (Fig. 6b). Both residual geoid and topography along the axis of the Laccadive Ridge show higher values and decrease on either side.

For GTR analysis, a polygon was selected to sample the Laccadive Ridge without including adjacent geological features such as seamounts, continental margin etc. so that results are not influenced by any artefacts. GTR is computed by taking the slope of the best-fitting least square regression line through the scatter plot of residual topography and geoid (Fig. 6c). The calculated GTR over the ridge is 0.44 m/km. In general, the GTR values are grouped into three ranges; (i) 0-2 m/km

indicating shallow compensation (ii) 2-6 m/km corresponds to thermal isostasy and (iii) >6 m/km indicating sub-lithospheric compensation supported by mantle convection (Sandwell and Mackenzie, 1989). Therefore, it is inferred that Laccadive Ridge is also compensated at shallow depth. Mishra et al. (2018) calculated GTR over the Laxmi Ridge and found a negative value of it (-1.98 m/km). They interpreted that the negative GTR over the Laxmi Ridge could be caused by shallow subsurface load (<20 km) with small wavelength (<200 km).

4.5. P-wave velocity structure

The long-range sonobuoy refraction stations L05, L07 on the Laxmi Ridge depict velocity-range 1.82 to 2.27 km/s in the first layer, 4.3 to 4.6 km/s in the second layer, 5.2 to 5.4 km/s in the third layer, 6.2 to 6.3 km/s in the fourth layer and 7.2 to 7.4 km/s in the fifth layer, whereas refraction station L08, L12 on the Laccadive Ridge display almost similar velocity structure, i.e. 1.65 to 2.12 km/s in the first layer, 4.2 to 4.4 km/s in the second layer, 5.6 to 5.7 km/s in the third layer, 6.3 km/s in the fourth layer and 7.2 to 7.3 km/s in the fifth layer (Table-3). Gupta et al. (2010) based on receiver function analysis categorized the crust of the Laccadive Ridge in P-wave velocity-ranges of 2.5-5 km/s, 5.4-5.8 km/s, 6.4-7.0 km/s and 7.3-7.6 km/s. These observations suggest that both the ridges have almost similar velocity structure. After compiling all the refraction data (Naini and Talwani, 1983) over the Laxmi, Laccadive ridges and the Eastern Basin five layers of P-wave velocity range 1.74-3.28 km/s, 4.1-4.9 km/s, 5.1-5.85 km/s, 6.1-6.6 km/s and 7.0-7.4 km/s are noticed. The layer with velocity-range 4.1-4.9 km/s is interpreted as flood basalt by Kumar and Chaubey (2019). The layers with velocities 5.1-5.85 km/s and 6.1-6.6 km/s are considered as continental crustal layers. These velocities do not represent typical upper continental and lower continental crustal layers; however, considering the tectonic history of the study area, the original crustal configuration might have been modified in geological past. The lowermost crustal layer of velocity 7.0-7.4 km/s is interpreted as high-density underplated layer.

4.6. Crustal models across the Laxmi and Laccadive ridges

To understand the crustal architecture under available geological and geophysical constraints, three transects (SK64-02, SK162-09 and SK162-13) across the Laxmi Ridge and two transects (SK12-08 and SK22-03) across the Laccadive Ridge (Fig. 3) have been selected for crustal structure modelling along which ship-borne free-air gravity, magnetic anomalies and bathymetry data are available. Along the transect SK12-08, multichannel seismic data is also available (Fig. 7). The gravity, magnetic and bathymetry data along these profiles are filtered using Gaussian filter of width 5km and then resampled at 0.4 km. Crustal structure derived from potential field data modelling is non-

unique; however, simultaneous modelling of gravity and magnetic data under the constraints from seismic data provide reliable crustal structure.

From all the compiled refraction data (Naini and Talwani, 1983), it is noticed that velocity in sedimentary layer varied from 1.74 km/s to 3.28 km/s. Beneath the sedimentary layer, the Western Basin is characterized by two layers with P-wave velocities of 5.4-5.75 km/s and 6.4-6.8 km/s, which represent oceanic layer-2 and layer-3, respectively. Based on refraction data, five-layered crustal structure is considered for both the ridges which includes sediments, flood basalt, crustal layer-1, crustal layer-2 and high-density underplated layer. Average P-wave velocity from the refraction data in these layers is calculated and converted to density (Table-1) using Brocher (2005) formula. The average P-wave velocity, corresponding density and magnetic parameters of these layers, incorporated in calculation are summarized in Table-1. In order to achieve a good fit between observed and calculated anomalies, several intrusive bodies have been introduced during integrated gravity and magnetic modelling. The presence of intrusions is also justified from the magnetic anomaly and tilt derivative map (Figs. 3 and 4). The locations of intrusions are fixed from these maps.

In a case of continental crust underneath the flood basalt, the magnetic signature will mainly be governed by flood basalt as the continental crust has negligible magnetization and susceptibility in comparison to the flood basalt. In a case of oceanic crust underneath the flood basalt, the magnetic response will be governed by both; however, influence of flood basalt will be relatively more because of its presence at a shallower depth than the underlying oceanic crust. In such cases other geophysical signatures are considered to model the crustal structure as crustal structure derived from potential field data modelling face problem of non-uniqueness. Therefore, in the present case, this problem is dealt with simultaneous modelling of gravity and magnetic data under the constraints from seismic data, which should provide a reliable crustal structure.

The transect SK64-02 passes through the E-W part of the Laxmi Ridge and extends for ~105 km from the Western Basin to the Gop Basin (Fig. 3). Along the transect, maximum igneous crustal thickness is ~16 km interpreted below the Laxmi Ridge (Fig. 8a). The Laxmi Ridge and the Gop Basin both are carpeted with flood basalt and intruded with volcanics. Magnetic polarities of the flood basalt and intrusions associated with the Laxmi Ridge are interpreted as reverse and normal, respectively. The Laxmi Ridge and the Gop Basin both are underplated with high-density material. Underplated layer below the ridge is thicker (~8.1 km) than that of the Gop Basin (~3.6 km). The Moho gradually decreases from ~20.6 km below the Laxmi Ridge to ~13.0 km below the Western Basin and ~14.6 km below the Gop Basin.

The transect SK162-09 is 200 km long and crosses the NW-SE segment of the Laxmi Ridge (Fig. 3). In accordance with the gravity anomaly trend, the transect shows a variation in the Moho (Fig. 8b). Depth to the Moho varies between 11.7 km (Western Basin) and 20.2 km (Laxmi Ridge). Maximum igneous crustal thickness of the Laxmi Ridge is ~15.4 km. The Laxmi Ridge and the Laxmi Basin both are underplated with high-density material. Maximum thickness of the underplated layer is ~7.0 km below the Laxmi Ridge and 3.1 km below the Laxmi Basin. Magmatic bodies in the form of a basaltic layer (reverse magnetic polarity) and intrusives (reverse and normal magnetic polarities) are also inferred along the profile. Maximum thickness of flood basalt is ~1.1 km over the Laxmi Ridge and ~2.0 km in the Laxmi Basin.

Transect SK162-13 passes through the southernmost block of the Laxmi Ridge from the Western Basin to the Laxmi Basin (Fig. 3). Maximum igneous crustal thickness and maximum depth to the Moho along this profile are inferred to be ~15.2 and 19.3 km, respectively below the Laxmi Ridge (Fig. 8c). The Laxmi Ridge and the Laxmi Basin both are carpeted with flood basalt which lies below the sediments. Maximum thickness of flood basalt is estimated to be ~1.6 over the Laxmi Ridge. There are three intrusive bodies of reverse magnetic polarity and one of normal magnetic polarity within the crust of the Laxmi Ridge. The Laxmi Ridge and Laxmi Basin both are underplated with high-density material. The estimated maximum thickness of underplated layer below the Laxmi Ridge and Laxmi Basin is ~8.6 and 3.4 km, respectively. The Moho gradually decreases from ~19.3 km below the Laxmi Ridge to ~12.3 km below the Western Basin and ~14.5 km below the Laxmi Basin.

Integrated gravity and magnetic modelling was also carried out along transect SK12-08 containing multichannel seismic data (Fig. 7) in addition to ship-borne bathymetry, magnetic and gravity data (Fig. 3). The multichannel seismic section along track SK12-08 has imaged the acoustic basement which is rugged and uneven (Fig 7). The basement high corresponding to the Laccadive Ridge is marked in Figure 7. Eastern flank of the Laccadive Ridge is associated with several normal faults which might be related with rifting. In addition, several intrusive bodies are also interpreted from the seismic data. In general, basement of the western flank of the Laccadive ridge has a gentle slope (~1:100) while that of the eastern part is nearly flat. From the integrated gravity and magnetic modelling, interpreted maximum igneous crustal thickness and the Moho depth below the Laccadive Ridge are 17.0 km and 20.7 km, respectively (Fig. 8d). Flood basalt of reverse polarity is spread over the ridge (at present lying beneath the sediments) and its thickness varies from 0.4 km to 2.0 km. Several intrusive bodies of reverse polarities intruded the crust of the ridge. Coral growth is

interpreted over the three intrusive bodies (Fig. 8d) which indicate that in the past, these intrusives were near the sea-surface and later subsided. High-density underplated layer is present below the ridge and it thickens eastward from ~4.7 km to ~8.5 km. Moho depth below the Western Basin is ~11.2 km which increases towards the Laccadive Ridge. Below the ridge, the Moho deepens eastward from 13.0 km to 20.7 km.

Transect SK22-03 traverses for 400 km from the Western Basin to the Laccadive Basin (Fig. 3). The ridge is carpeted with flood basalt which belongs to reverse magnetic polarity. Thickness of flood basalt is variable with minimum and maximum values of 0.8 km and 2.1 km, respectively. Two intrusive bodies of normal and two of reverse magnetic polarity are also observed within the crust of the ridge (Fig. 8e). Coral growth is interpreted over the two intrusive bodies (Fig. 8e). The ridge is underplated by high-density material and its maximum and minimum thicknesses are ~8.6 km and 2.8 km, respectively. The Moho depth varies from 10.8 km (below adjacent Western Basin) to ~20.0 km (below the Laccadive Ridge).

5. Discussion

5.1. Crustal architecture of the Laxmi and Laccadive ridges

Best fit crustal models across the Laxmi and Laccadive ridges reveal similarity in their crustal layers. Major crustal units of the ridges are sediments, flood basalt, crustal layer-1, crustal layer-2 and high-density underplated layer. Crustal models of both the ridges indicate that the flood basalts (basaltic layer) of variable thickness are present below the Tertiary sediments and are associated with reverse magnetic polarity. Several magmatic intrusive bodies of both magnetic polarities (normal and reverse) are also present within crust of the ridges. Both the ridges exhibit predominance of intrusions of reverse polarity. Presence of flood basalt (except on some isolated basement high features) on the entire northwestern continental margin of India including the Laxmi Ridge, is also reported in a recent study by Kumar and Chaubey (2019). Similarly, presence of basalt over the Laccadive Ridge has also been reported earlier by previous researchers (Ajay et al., 2010; Nair et al., 2013). Earlier studies indicated underplating below the Laxmi Ridge (Naini and Talwani 1983; Minshull et al., 2008; Mishra et al., 2018) and the Laccadive Ridge (Ajay et al., 2010; Gupta et al., 2010). Subsurface to surface load ratio for the Laccadive Ridge is 0.7 (computed in the present study) and for the Laxmi Ridge, it is 0.8 (Mishra et al., 2018) which support presence of a huge underplating layer below the ridges. All crustal models across both the ridges derived through integrated gravity and magnetic modelling also displayed a thick layer of underplating as well as intrusive bodies. Further, presence of rotated fault block system, continental basalt (Murty et al.,

1999; Kothari et al., 2001), seaward dipping reflector (Ajay et al., 2010) support continental origin of the Laccadive Ridge which is later affected by magmatic activity. Therefore, based on the results of the present study and existing knowledge, we interpret the crustal nature of the Laxmi and Laccadive ridges is of continental origin which is heavily intruded. Both the ridges are carpeted with flood basalt (at present lying beneath the sediments) and underplated by a high-density material all along its length.

Elastic plate thickness of the Laccadive Ridge obtained through coherence analysis is about 3 km which is in good accordance with the values (2-5 km) derived through different methods in previous studies (Ashalatha et al., 1991; Bansal et al., 2005; Tiwari et al., 2007; Chaubey et al., 2008). The low value of T_e implies that the Laccadive Ridge is locally compensated and lithosphere is elastically weak beneath it. The Laccadive Ridge has witnessed two main rifting episodes (i) rifting between Madagascar and Laccadive-India during mid-Cretaceous and (ii) rifting between Laccadive Ridge and India, at its western and eastern ends, respectively. The crustal setup got modified during these rifting processes. Also, the whole region came into contact of the Réunion hotspot during 67 Ma to 60 Ma and got extensively deformed. Subsurface to surface load ratio $F = 0.7$ connotes that subsurface processes have contributed significantly in reducing the lithospheric strength. Therefore, it is interpreted that rifting processes and the Réunion hotspot were two major factors due to which lithosphere beneath the Laccadive Ridge became weak in spite of being continental in nature. The Laxmi Ridge also displays similar characteristics, i.e. almost the same T_e and F value as reported in Mishra et al. (2018). The Laxmi Ridge too had undergone two phases of rifting on its eastern and western side. Besides, its crustal setup was also altered by the Réunion hotspot during the Early Tertiary.

5.2. Magmatic activity along the Laxmi and Laccadive ridges

Magnetic anomaly signatures and the crustal models derived through integrated gravity and magnetic modelling have shown that both the ridges are carpeted with flood basalt as well as intruded with volcanics. The flood basalt belongs to reverse magnetic polarity and intrusive bodies within the crust of the ridges belong to both normal as well as reverse polarities. Presence of both the magnetic polarities indicates that the volcanics are placed during different geological time. Tectonic history of the region suggests that the Réunion and Marion hotspots are the major sources of volcanism. The Réunion hotspot erupted during magnetic Chron 29n to Chron 30n and most of the volcanism occurred within 0.8 Myr which corresponds to Chron 29r (Courillot et al., 1986). Flood basalt, interpreted in different crustal models of the Laxmi Ridge is of reverse magnetic polarity which is in

line with the reported fact. The normal and reverse volcanic intrusions within the crust of the Laxmi Ridge might be placed during either Chron 29n or Chron 30n and Chron 29r, respectively.

Age of the flood basalt or intrusions of the Laccadive Ridge is difficult to speculate because it was impacted not only by the Marion hotspot during India-Madagascar separation but also by the R union hotspot during the Early Tertiary. Estimated ages of recovered basalt from drill-well over Padua Bank are 102 Ma and 60 Ma (Kothari et al., 2001). The 102 Ma age may be associated with the volcanism from Marion hotspot during rifting between India and Madagascar. However, the 60 Ma age corresponds with the R union hotspot related volcanism. These observations indicate that the Laccadive Ridge experienced magmatism at least from two sources. Therefore, it can be concluded that both the ridges have experienced volcanic activity in the geological past.

5.3. Continuation of the Laxmi Ridge towards the Laccadive Ridge

The seismic sections along RE11 (Krishna et al., 2006); RE13 (Ajay, 2011); RC1707_64, V3408_5 (NCEI); and SK12-08 (Figs. 7 and 9) are passing near the junction of the Laxmi and Laccadive ridges. The seismic section along V3408_5 passing across the southernmost part of the Laxmi Ridge clearly depicts basement high (Fig. 9). This basement high is further continued southeastward and can be seen in seismic sections along RC1707_64 (Fig. 9) passing through transition zone between the Laxmi and Laccadive ridges as well as in sections RE13 (Fig. 9) and SK12-08 (Figs. 7 and 9) passing through the northernmost part of the Laccadive Ridge. These observations suggest that the basement high corresponding to the Laxmi Ridge is further continued southeastwards and conjoins with the northwestern flank of the Laccadive Ridge.

Further, there are several similar characteristics, which are observed by analyzing the results of present and previous studies on both the ridges. (i) Both the ridges have similar crustal structure as inferred through integrated gravity and magnetic modelling, (ii) both the ridges are interpreted as continental fragments, (iii) both the ridges had experienced stretching and rifting at its eastern and western end in the geological past, (iv) elastic plate thickness of both the ridges is low and in the same range (~3-4 km) (v) both the ridges are underplated with almost same thickness of high-density material (vi) both the ridges are carpeted with flood basalt as well as heavily intruded (vii) The NW-SE segment of the Laxmi Ridge reveals several linear features which are limited within its boundary and having NW-SE trend (Fig. 9). Also, the northwestern part of the Laccadive Ridge depicts NW-SE trending structural features similar to that of the Laxmi Ridge (Fig. 9). These structural lineaments do suggest a similarity between northwestern flank of the Laccadive Ridge and NW-SE segment of the Laxmi Ridge. In addition, the northwestern flank of the Laccadive Ridge is associated

with a free-air gravity anomaly low which is falling in continuation of the gravity anomaly low of the Laxmi Ridge. Also from the tilt derivative map, Laxmi Ridge seems to be continued structurally southeastward and conjoins western part of the Laccadive Ridge (Fig. 9). Naini and Talwani (1983) were also of the opinion that the Laxmi and Laccadive ridges have similar nature, and morphologically the former one is the northwestward continuation of the latter one. However, Todal and Edholm (1998), based on crustal density models, inferred that the Laxmi and Laccadive ridges are separate features. Results of present study advocate similar crustal model for both ridges, which is further supported by the velocity model as observed on refraction stations L08, L12 on the Laccadive and L05, L06 on the Laxmi ridges (Fig. 9). On the basis of above results and discussion, we believe that the Laxmi Ridge continues southeastward and unites with the northwestern part of the Laccadive Ridge.

6. Conclusions

Analyses and results of geophysical data through integrated approach have provided a new understanding of crustal structure, subsurface loading and interrelationship of the Laxmi and Laccadive ridges. Major findings of the present study are summarized as follows:

- i. The effective elastic plate thickness of the Laccadive Ridge, as determined from coherence analysis between mantle Bouguer anomaly and residual bathymetry, is about 3 km with subsurface to surface load ratio 0.7.
- ii. The Laccadive Ridge is compensated locally and lithosphere is elastically weak beneath it. Various rifting processes between India, Madagascar and Laccadive; and reheating by the Réunion hotspot are the possible cause of weak lithosphere.
- iii. Both the Laxmi and Laccadive ridges are carpeted with flood basalt as well as heavily intruded. The flood basalt and most of the intrusive bodies belong to reverse magnetic polarity, while few intrusions belong to normal magnetic polarity.
- iv. Both the ridges are underplated all along its length and its maximum thickness reaches about 8.6 km.
- v. Both the ridges have similar crustal model and of continental origin. The Laxmi Ridge continues southeastward and conjoins with the northwestern part of the Laccadive Ridge.

Acknowledgements

The authors are thankful to Prof. Sunil Kumar Singh, Director, CSIR-National Institute of Oceanography, Goa for support and encouragement during course of this work. Figures were prepared using GMT software of Wessel and Smith (1998). The authors are grateful to Prof. Mei-Fu

Zhou, Editor-in-Chief JAES, Prof. Manoj Pandit, Editor, JAES and two anonymous reviewers for their comments and suggestions. AM and PK acknowledge the Council of Scientific and Industrial Research, New Delhi and KMD acknowledges University Grant Commission, New Delhi for financial support as JRF & SRF. This is NIO contribution no. xxx.

References

Ajay, K.K., Chaubey, A.K., Krishna, K.S., Rao, D.G., Sar, D., 2010. Seaward dipping reflectors along the SW continental margin of India: evidence for volcanic passive margin. *J. Earth Syst. Sci.* 119, 803-813.

Ajay, K.K., 2011. Seismic stratigraphy, sedimentation history and tectonics of the southwest continental margin of India. PhD thesis, Goa University.

Amante, C., Eakins, B.W., 2009. ETOPO1 1 Arc-Minute Global Relief Model: Procedures, Data Sources and Analysis. NOAA Technical Memorandum NESDIS NGDC-24. National Geophysical Data Center, NOAA. <http://dx.doi.org/10.7289/V5C8276M>.

Arora, K., Tiwari, V.M., Singh, B., Mishra, D.C., Grevemeyer, I., 2012. Three dimensional lithospheric structure of the western continental margin of India constrained from gravity modelling: implication for tectonic evolution. *Geophys. J. Int.* 190, 131-150.

Ashalatha, B., Subrahmanyam, C., Singh, R.N., 1991. Origin and compensation of Chagos-Laccadive ridge, Indian ocean, from admittance analysis of gravity and bathymetry data. *Earth Planet. Sci. Lett.* 105, 47-54.

Avraham, Z.B. and Bunce, E.T., 1977. Geophysical study of the Chagos-Laccadive Ridge, Indian Ocean. *J. Geophys. Res.* 82, 1295-1305.

Bansal, A.R., Fairhead, J.D., Green, C.M., Fletcher, K.M.U., 2005. Revised gravity for offshore India and the isostatic compensation of submarine features. *Tectonophysics* 404, 1-22.

Bhattacharya, G.C., Chaubey, A.K., 2001. Western Indian Ocean-a glimpse of the tectonic scenario. In: Sengupta R, Desa, E. (Eds.), *The Indian Ocean-a perspective*. Oxford & IBH Pub. Company Ltd., Delhi, pp. 691-729.

Bhattacharya, G.C., Chaubey, A.K., Murty, G.P.S., Srinivas, K., Sarma, K.V.L.N.S., Subrahmanyam, V., Krishna, K.S., 1994. Evidence for seafloor spreading in the Laxmi Basin, northeastern Arabian Sea. *Earth Planet. Sci. Lett.* 125, 211-220.

Bhattacharya, G.C., Yatheesh, V., 2015. Plate-tectonic evolution of the deep ocean basins adjoining the Western continental margin of India-A proposed model for the early opening scenario. In: Mukherjee, S. (Ed.), *Petroleum Geosciences: Indian Contexts*. Springer International Publishing, Cham, pp. 1-61.

Bowin, C., 1983. Depth of principal mass anomalies contributing to the earth's geoidal undulations and gravity anomalies. *Mar. Geod.* 7, 61-100.

Brocher, T.M., 2005. Empirical relations between elastic wavespeeds and density in the Earth's crust. *Bull. Seismol. Soc. Am.* 95, 2081-2092.

Chaubey, A.K., Bhattacharya, G.C., Rao, D.G., 1995. Seafloor spreading magnetic anomalies in the southeastern Arabian Sea. *Mar. Geol.*, 128, 105-114.

Chaubey, A.K., Bhattacharya, G.C., Murty, G.P.S., Srinivas, K., Ramprasad, T., Rao, D.G., 1998. Early Tertiary seafloor spreading magnetic anomalies and paleo-propagators in the northern Arabian Sea. *Earth Planet. Sci. Lett.* 154, 41-52.

- Chaubey, A., Gopala Rao, D., Srinivas, K., Ramprasad, T., Ramana, M., Subrahmanyam, V., 2002a. Analyses of multichannel seismic reflection, gravity and magnetic data along a regional profile across the central-western continental margin of India. *Mar. Geol.* 182, 303-323.
- Chaubey, A.K., Dymant, J., Bhattacharya, G.C., Royer, J.-Y., Srinivas, K., Yatheesh, V., 2002b. Paleogene magnetic isochrons and palaeo-propagators in the Arabian and Eastern Somali basins, NW Indian Ocean. *Geol. Soc. Lond., Spec. Publ.* 195, 71-85.
- Chaubey, A.K., Srinivas, K., Ashalatha, B., Rao, D.G., 2008. Isostatic response of the Laccadive Ridge from admittance analysis of gravity and bathymetry data. *J. Geodyn.* 46, 10-20.
- Courtillot, V., Besse, J., Vandamme, D., Montigny, R., Jaeger, J.J., Cappetta, H., 1986. Deccan flood basalts at the Cretaceous/Tertiary boundary? *Earth Planet. Sci. Lett.* 80(3-4), 361-374.
- Crough, S.T., 1983. The correction for sediment loading on the seafloor. *J. Geophys. Res. Solid Earth* 88, 6449-6454.
- Divins, D.L., 2003. Total Sediment Thickness of the World's Oceans & Marginal Seas. NOAA National Geophysical Data Center, Boulder, CO.
- Duncan, R.A., 1981. Hotspots in the southern Oceans: An absolute frame of reference motion of the Gondwana Continents. *Tectonophysics* 74, 29-42.
- Duncan, R.A., 1990. The volcanic record of the Réunion hotspot. In: R.A. Duncan, J. Backman, L.C. Peterson et al. (Eds), *Proc. ODP, Sci. Results.*, 115:College Station, TX (Ocean Drilling Program), 3-10.
- Forsyth, D.W., 1985. Subsurface loading and estimates of the flexural rigidity of continental lithosphere. *J. Geophys. Res. Solid Earth* 90, 12623-12632.
- Fisher, R.L., Sclater, J.G., McKenzie, D.P., 1971. The evolution of the Central Indian Ridge, Western Indian Ocean. *Geol. Soc. Am. Bull.* 82, 553-562.
- Gupta, S., Mishra, S., Rai, S.S., 2010. Magmatic underplating of crust beneath the Laccadive Island, NW Indian Ocean. *Geophys. J. Int.* 183, 536-542.
- Haxby, W.F., Turcotte, D.L., 1978. On isostatic geoid anomalies. *J. Geophys. Res. Solid Earth* 83, 5473-5478.
- Kothari, V., Waraich, R.S., Dirghangi, R.S., Baruah, R.M., Lal, N.K., Zutshi, P.L., 2001. A reassessment of the hydrocarbon prospectivity of Kerala-Konkan deep water basin, western offshore, India. In: A.K. Bhatnagar (Ed.), *Hydrocarbon Exploration. Proc. Fifth Int. Pet. Conf. and Exbn, Petrotech-2001.*
- Krishna, K.S., Rao, D.G., Sar, D., 2006. Nature of the crust in the Laxmi Basin (14°-20°N), western continental margin of India. *Tectonics* 25. <http://dx.doi.org/10.1029/2004tc001747>.
- Kumar P., Chaubey A.K., 2019. Extension of flood basalt on the northwestern continental margin of India. *J. Earth Syst. Sci.* 128:81. <https://doi.org/10.1007/s12040-019-1089-6>.
- Luis, J.F., Neves, M.C., 2006. The isostatic compensation of the Azores Plateau: a 3D admittance and coherence analysis. *J. Volcanol. Geotherm. Res.* 156, 10-22.

- McKenzie, D., Sclater, J.G., 1971. The evolution of the Indian Ocean since the Late Cretaceous. *Geophys. J. R. Astron. Soc.* 25, 437-528.
- Miller, H.G., Singh, V., 1994. Potential field tilt-a new concept for location of potential field sources. *J. Appl. Geophys.* 32, 213-217.
- Minshull, T.A., Lane, C.I., Collier, J.S., Whitmarsh, R.B., 2008. The relationship between rifting and magmatism in the northeastern Arabian Sea. *Nat. Geosci.* 1, 463-467.
- Mishra, A., Chaubey, A.K., Sreejith, K.M., Kumar, S., 2018. Crustal underplating and effective elastic plate thickness of the Laxmi Ridge, northern Arabian Sea. *Tectonophysics* 744, 82-92.
- Misra, A.A., Sinha, N., Mukherjee, S., 2015. Repeat ridge jumps and microcontinent separation: insights from NE Arabian Sea. *Mar. Pet. Geol.* 59, 406-428.
- Murty, A.V.S., Arasu, R.T., Dhanawat, B.S., Subrahmanyam, V.S.R., 1999. Some aspects of deepwater exploration in the light of new evidences in the western Indian offshore. In: Bhatnagar, A.K. (Ed.), *Hydrocarbon Exploration. Papers of the Third International Petroleum Conference and Exhibition, Petrotech- 99*, Thompson, Faridabad, India, pp 457-463.
- Naini, B.R., Talwani, M., 1983. Structural framework and the evolutionary history of the continental margin of western India. In: Watkins, J.S., Drake, C.L. (Eds.), *Studies in Continental Margin Geology Am. Assoc. Pet. Geol. Mem.* 34, 167-191.
- Nair, N., Anand, S.P., Rajaram, M., 2013. Tectonic framework of Laccadive Ridge in Western Continental Margin of India. *Mar. Geol.* 346, 79-90.
- Nair, N., Anand, S., Rajaram, M., Rao, P.R., 2015. A relook into the crustal architecture of Laxmi Ridge, northeastern Arabian Sea from geopotential data. *J. Earth Syst. Sci.* 124, 613-630.
- Narain, H., Kaila, K.L., Verma, R.K., 1968. Continental margins of India. *Can. J. Earth Sci.* 5, 1051-1065.
- Pandey, O.P., Agrawal, P.K., Negi, J.G., 1995. Lithospheric structure beneath Laxmi Ridge and late Cretaceous geodynamic events. *Geo-Mar. Lett.* 15, 85-91.
- Parker, R.L., 1972. The rapid calculation of potential anomalies. *Geophys. J. Int.* 31, 447-455.
- Radhakrishna, M., Verma, R.K., Purushotham, A.K., 2002. Lithospheric structure below the eastern Arabian Sea and adjoining West Coast of India based on integrated analysis of gravity and seismic data. *Mar. Geophys. Res.* 23, 25-42.
- Ramana, M.V., Desa, M.A., Ramprasad, T., 2015. Re-examination of geophysical data off Northwest India: Implications to the Late Cretaceous plate tectonics between India and Africa. *Mar. Geol.* 365, 36-51.
- Rao, D.G., Paropkari, A., Krishna, K., Chaubey, A., Ajay, K., Kodagali, V., 2010. Bathymetric highs in the mid-slope region of the western continental margin of India-Structure and mode of origin. *Mar. Geol.* 276, 58-70.
- Reid, A.B., Allsop, J.M., Granser, H., Millett, A.J., Somerton, I.W., 1990. Magnetic interpretation in three dimensions using Euler deconvolution. *Geophys.* 55, 80-91.

- Richards, M.A., Duncan, R.A. and Courtillot, V.E., 1989. Flood basalts and hotspot tracks: plume heads and tails. *Science* 246, 103-107.
- Sandwell, D.T., Mackenzie, K.R., 1989. Geoid height versus topography for oceanic plateaus and swells. *J. Geophys. Res. Solid Earth* 94, 7403-7418.
- Sandwell, D.T., Müller, R.D., Smith, W.H.F., Garcia, E., Francis, R., 2014. New global marine gravity model from CryoSat-2 and Jason-1 reveals buried tectonic structure. *Science* 346, 65–67.
- Sandwell, D.T., Renkin, M.L., 1988. Compensation of swells and plateaus in the north Pacific: no direct evidence for mantle convection. *J. Geophys. Res. Solid Earth* 93, 2775-2783.
- Singh, A.P., 1999. The deep crustal accretion beneath the Laxmi Ridge in the northeastern Arabian Sea: the plume model again. *J. Geodyn.* 27, 609-622.
- Shipboard Scientific Party, 1988. Site 715. In: R.A. Duncan and others (Editors), *Proceedings Ocean Drilling Program*, pp.917-946.
- Sreejith, K.M., Rajesh, S., Majumdar, T.J., Srinivasa Rao, G., Radhakrishna, M., Krishna, K.S., Rajawat, A.S., 2013. High-resolution residual geoid and gravity anomaly data of the northern Indian Ocean - an input to geological understanding. *J. Asian Earth Sci.* 62, 616-626.
- Talwani, M., Reif, C., 1998. Laxmi Ridge - a continental sliver in the Arabian Sea. *Mar. Geophys. Res.* 20, 259-271.
- Talwani, M., Worzel, J.L., Landisman, M., 1959. Rapid gravity computations for twodimensional bodies with application to the Mendocino submarine fracture zone. *J. Geophys. Res.* 64, 49-59.
- Tiwari, V.M., Grevemeyer, I., Singh, B., Phipps Morgan, J., 2007. Variation of effective elastic thickness and melt production along the Deccan-Réunion hotspot track. *Earth Planet. Sci. Lett.* 264, 9-21.
- Total, A., Edholm, O., 1998. Continental margin off Western India and Deccan Large Igneous Province. *Mar. Geophys. Res.* 20, 273-291.
- Wessel, P., 2010. Tools for analyzing intersecting tracks: The x2sys package. *Computers & Geosciences* 36, 348-354.
- Wessel, P., Smith, W.H.F., 1998. New, improved version of generic mapping tools released. *EOS Trans. Am. Geophys. Union* 79, 579-579.
- Whitmarsh, R.B., 1974. Some aspects of plate tectonics in the Arabian Sea. In: R.B. Whitmarsh, O.E. Weser, D.A. Ross, et al. (Eds), *Initial Reports of the Deep Sea Drilling Project*, Washington (U.S. Govt. Printing Office). 23, 527-535.
- Won, I.J., Bevis, M., 1987. Computing the gravitational and magnetic anomalies due to a polygon; algorithms and Fortran subroutines. *Geophysics* 52, 232-238.

Table 1 Average P-wave velocity in different crustal layers. Density for each layer is calculated using Brocher (2005) formula.

Crustal Layers	Average velocity (km/s)	Density (g/cm ³)	Susceptibility (CGS unit)	Remanent magnetization (emu/cm ³)
Sediments	2.73	2.20	---	---
Flood Basalt	4.50	2.46	0.001-0.003	0.001-0.007
Crustal Layer-1	5.43	2.60	---	---
Crustal Layer-2	6.30	2.77	---	---
Underplating	7.20	3.02	---	---
Oceanic Layer-2	5.51	2.62	0.001-0.003	0.001-0.007
Oceanic Layer-3	6.67	2.88	0.001-0.002	0.001-0.003
Mantle	8.10	3.33	---	---

Table 2 Model parameters used for calculation of theoretical coherence.

Parameter	Notation	Value
Density of sea-water	ρ_w	1.03 g/cm ³
Density of crust	ρ_c	2.70 g/cm ³
Density of mantle	ρ_m	3.30 g/cm ³
Young's modulus	E	100 Gpa
Poisson's ratio	σ	0.25
Acceleration due to gravity	g	9.81 m/s ²

Table 3 P-wave velocity in different crustal layers of the Laxmi and Laccadive ridges. V_p: P-wave velocity in km/s; T: Thickness in km; Ref.: Refraction; W.D: Water depth.

Name of feature	Ref. Stations	W. D. (km)	First Layer		Second Layer		Third Layer		Fourth Layer		Fifth Layer	
			V _p	T	V _p	T	V _p	T	V _p	T	V _p	T
Laxmi Ridge	L05V34	3.136	2.05	0.67	4.30	0.73	5.40	3.51	6.20	4.13	7.20	10.70
	L07V34	3.779	2.04	0.70	4.60	1.71	5.20	1.07	6.30	3.24	7.40	5.79
Laccadive Ridge	L08V34	2.135	1.89	0.83	4.40	0.66	5.60	1.49	6.30	4.69	7.20	8.40
	L12V34	3.628	2.00	0.43	4.20	1.70	5.70	1.93	6.30	1.84	7.30	7.99

Figure captions

Fig. 1 Generalized map of the western continental margin of India and adjacent ocean basins, depicting bathymetric contours (in meters), magnetic isochrons (coloured blocks), pseudofaults (blue lines), fracture zones (thin dashed lines) in the Arabian Basin (Chaubey et al., 2002b). Thin green and magenta lines represent magnetic lineation in the Laxmi and Gop basins identified by Bhattacharya and Yatheesh (2015) and Ramana et al. (2015), respectively. Thick dark-red and green curves represent the R union hotspot track (Shipboard Scientific Party, 1988) and the Laxmi Ridge gravity low, respectively. Dark-red stars denote the IODP and DSDP drilled sites. Study area is shown with dashed-black polygon and encompasses two prominent aseismic Laxmi and Laccadive ridges. R: Raman Seamount, P: Panikkar Seamount, W: Wadia Guyot.

Fig. 2 Map showing compiled ship-borne geophysical data (Seismic-S, Bathymetry-B, Gravity-G, Magnetic-M) along the tracks shown with different colours utilized in the present study. Red lines represent tracks along which SBGM data are available; Blue line represent tracks along which BGM data are available; Green line represent tracks along which BM data are available; Magenta lines correspond to the tracks along which published seismic sections (Krishna et al., 2006; Ajay, 2011; Misra et al., 2015), and orange lines represent tracks along which single-channel seismic section from NCEI are compiled. Dark-red circle denotes the refraction stations and Dark-red stars denote the IODP and DSDP drilled sites. Free-air gravity anomaly contours are drawn in background for reference. Study area is shown with black polygon.

Fig. 3 Map of tilt angle computed from free-air gravity anomaly. Solid black-square represent edge/boundary of the Laxmi and Laccadive ridges determined from seismic sections. Final boundaries of the Laxmi and Laccadive ridges, determined in present study are shown with black curve. Transition zone between both the ridges is shown with red lines. Black solid lines represent transects along which integrated gravity and magnetic anomaly modelling is carried out. R: Raman Seamount, P: Panikkar Seamount, W: Wadia Guyot.

Fig. 4 (a) 3D Euler solutions obtained over study area for Structural Index (SI) = 0, are plotted on the magnetic anomaly map of the study area. **(b)** Interpreted lineaments corresponding to fault/contacts from 3D Euler solutions obtained for SI = 0 and are shown with black lines. Boundaries of the Laxmi and Laccadive ridges are shown with dark-red curve.

Fig. 5 (a) Plot of observed coherence (red star with error-bar) between MBA and residual bathymetry, and theoretical coherence curves (blue) for T_e values 2, 3, 5 and 7 km assuming

$F=0.7$, **(b)** Root Mean Square (RMS) plot of the misfit between theoretical and observed coherence as a function of T_e and F . Black star shows minimum value of RMS which corresponds to $T_e=3.0$ km and $F=0.7$. The green curve in coherence plot corresponds to the best fit $T_e=3.0$ km and $F=0.7$.

Fig. 6 (a) Residual geoid anomaly over the Laccadive Ridge, calculated by filtering the geoid in wavelength-band 330-4000 km. **(b)** Residual topography calculated by filtering corrected bathymetry in wavelength-band 330-4000 km. **(c)** Scatter plot between residual geoid and residual topography in wavelength-band 330-4000 km; black line is the best fit line which gives geoid to topography ratio (GTR) for the Laccadive Ridge. The boundary of the Laccadive Ridge in (a) and (b) has been shown with black color curve.

Fig. 7 Seismic section along track SK12-08 (see Figs. 2 and 3 for location). Basement is shown with orange colour. Places of intrusions are indicated with upward arrow. TWT: Two Way Travel-time.

Fig. 8 Crustal models derived through integrated gravity and magnetic forward modelling under constraints from published crustal velocity and nearby seismic reflection data. **(a)** Crustal model along track SK64-02 (top) and crustal layers legends (bottom), **(b)** Crustal model along track SK162-09, **(c)** Crustal model along track SK162-13, **(d)** Crustal model along track SK12-08, and **(e)** Crustal model along track SK22-03. Parameters used in synthetic gravity and magnetic anomaly computations are listed in Table-1. For reversely magnetized bodies inclination is $+50^\circ$ and declination is $+130^\circ$. For normally magnetized bodies inclination is -50° and declination is -40° . D: Density in g/cm^3 ; FAA: Free-Air gravity Anomaly; MA: Magnetic Anomaly; RMSE: Root Mean Square Error.

Fig. 9 Map of tilt angle of free-air gravity anomaly of the Eastern Arabian Sea. Seismic sections along the track-lines (maroon lines) falling in transition zone, are shown in inset figures. Boundaries of the Laxmi and Laccadive ridges are shown with thin black curve. Black circles denote refraction stations. Northwestern part of the Laccadive Ridge (bounded between dashed black line and the northwestern boundary of the Laccadive Ridge) has NW-SE structural lineaments (marked with solid black lines) similar to that of the NW-SE segment of the Laxmi Ridge. Continuation of the Laxmi Ridge towards the Laccadive Ridge is shown with black dotted lines.

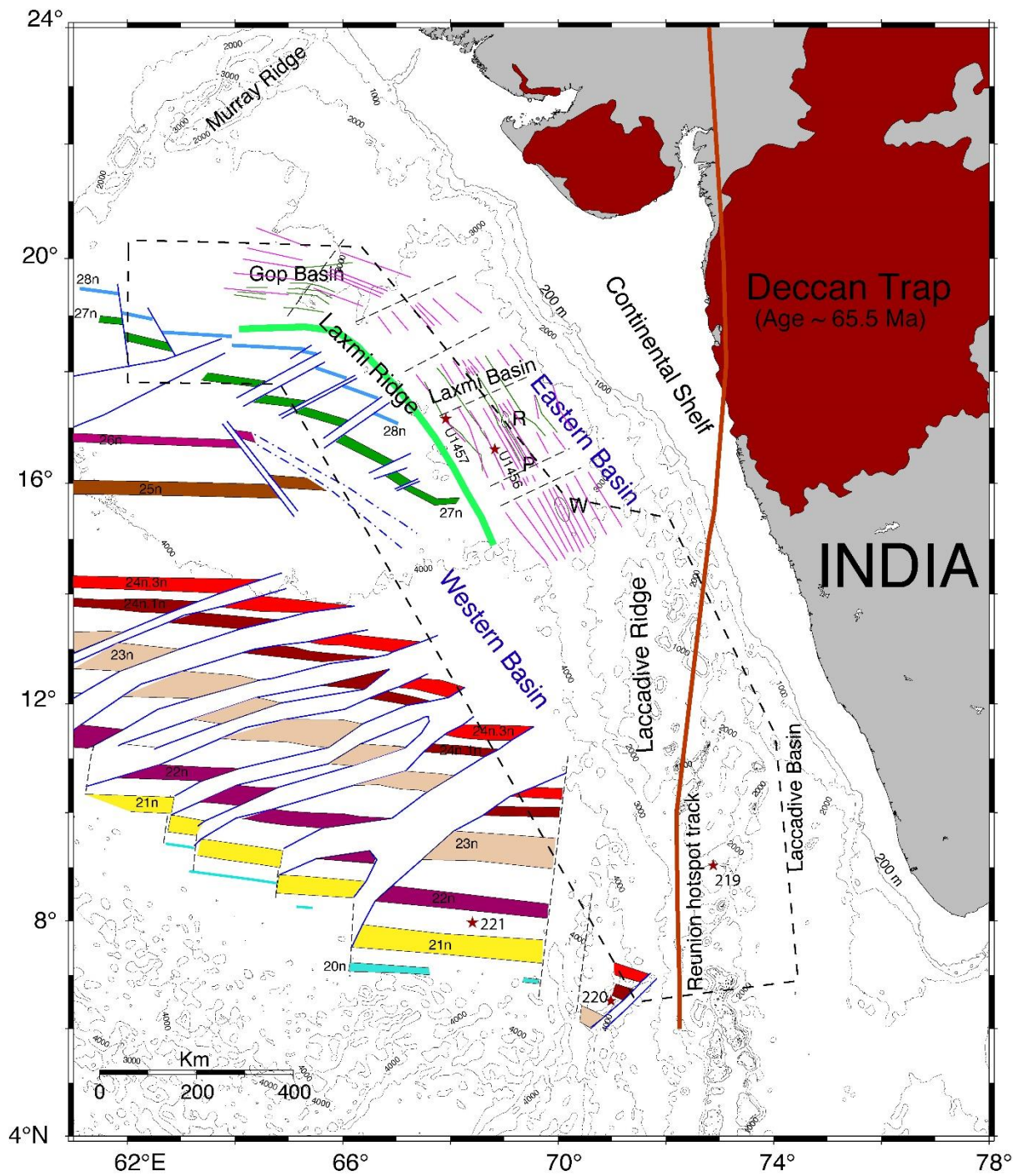


Fig. 1

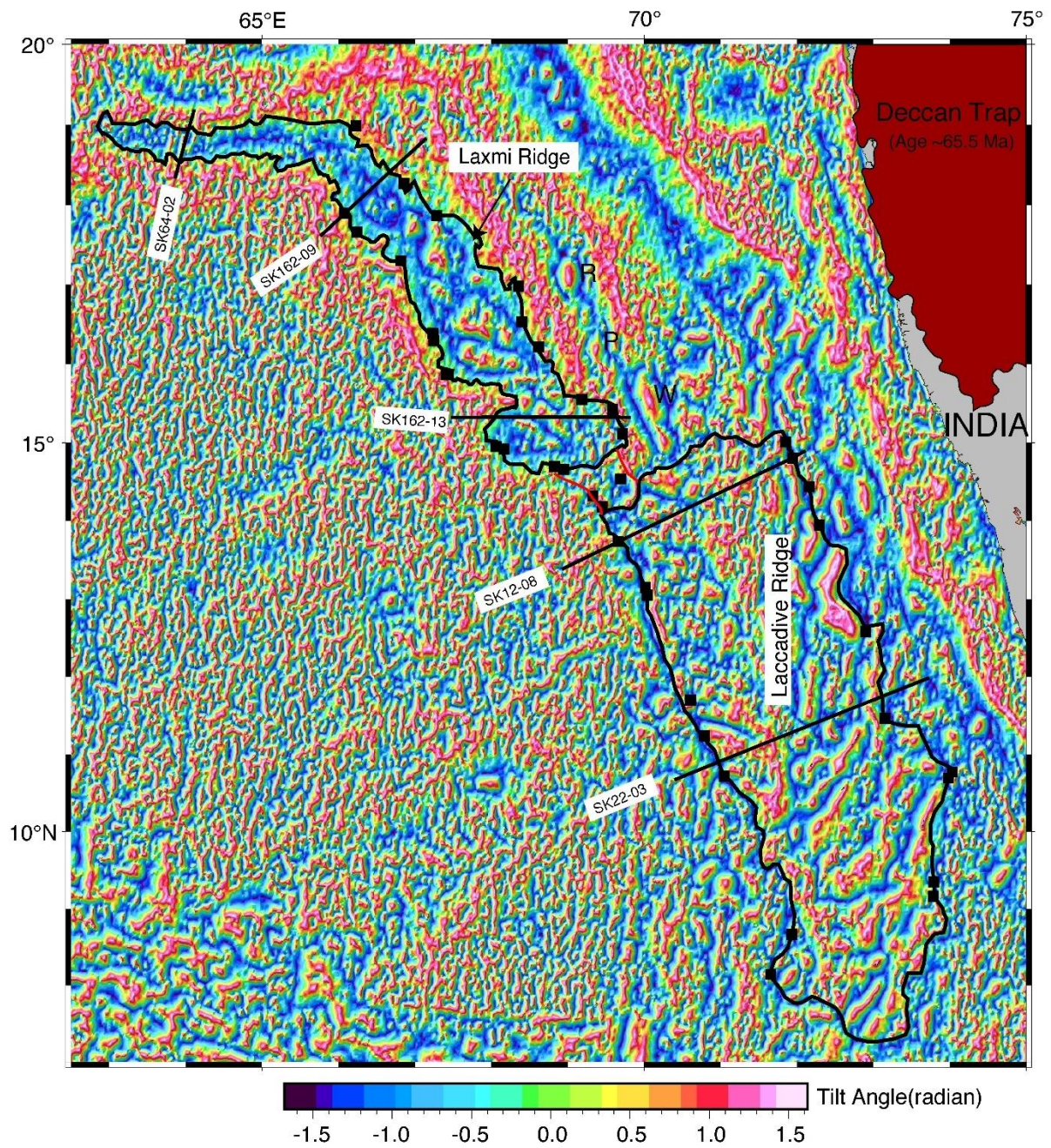


Fig. 3

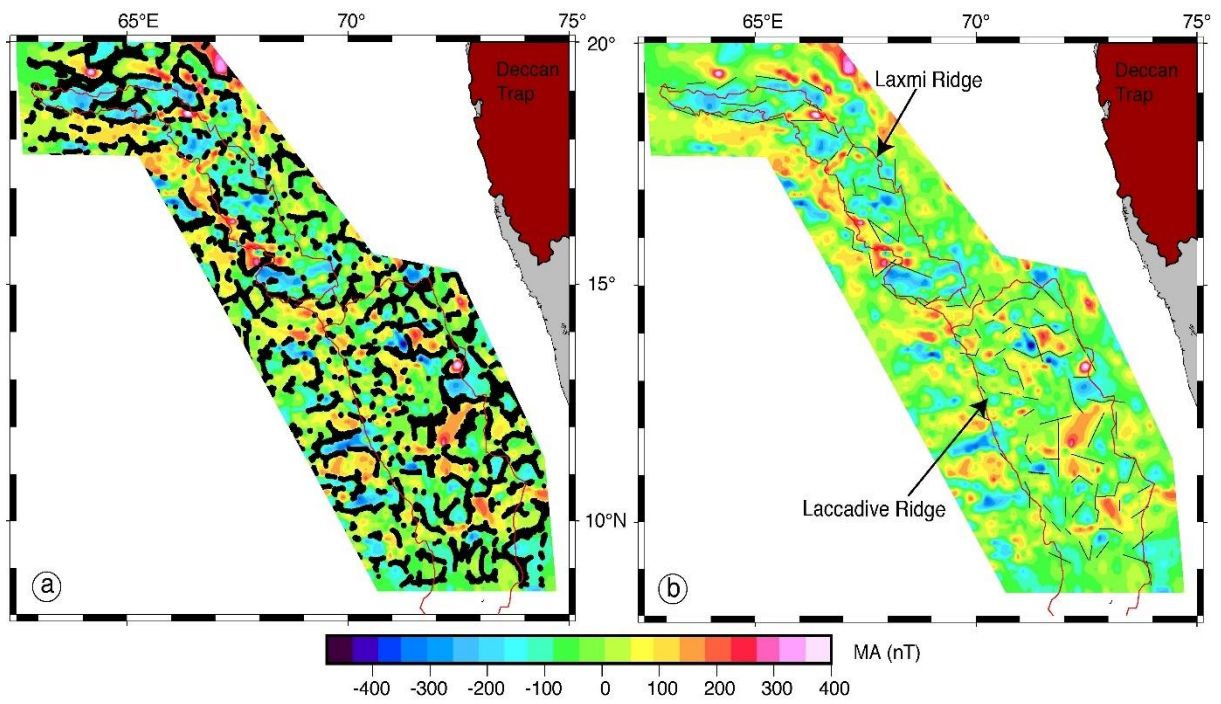


Fig. 4

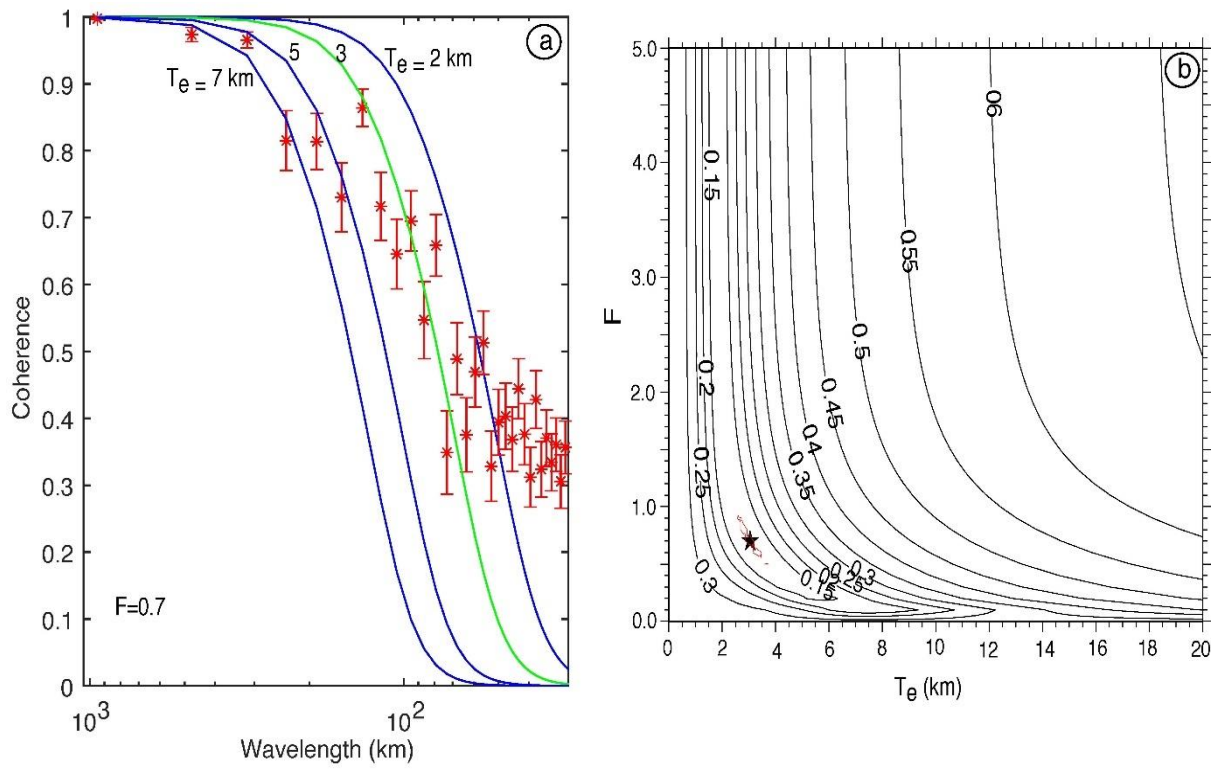


Fig. 5

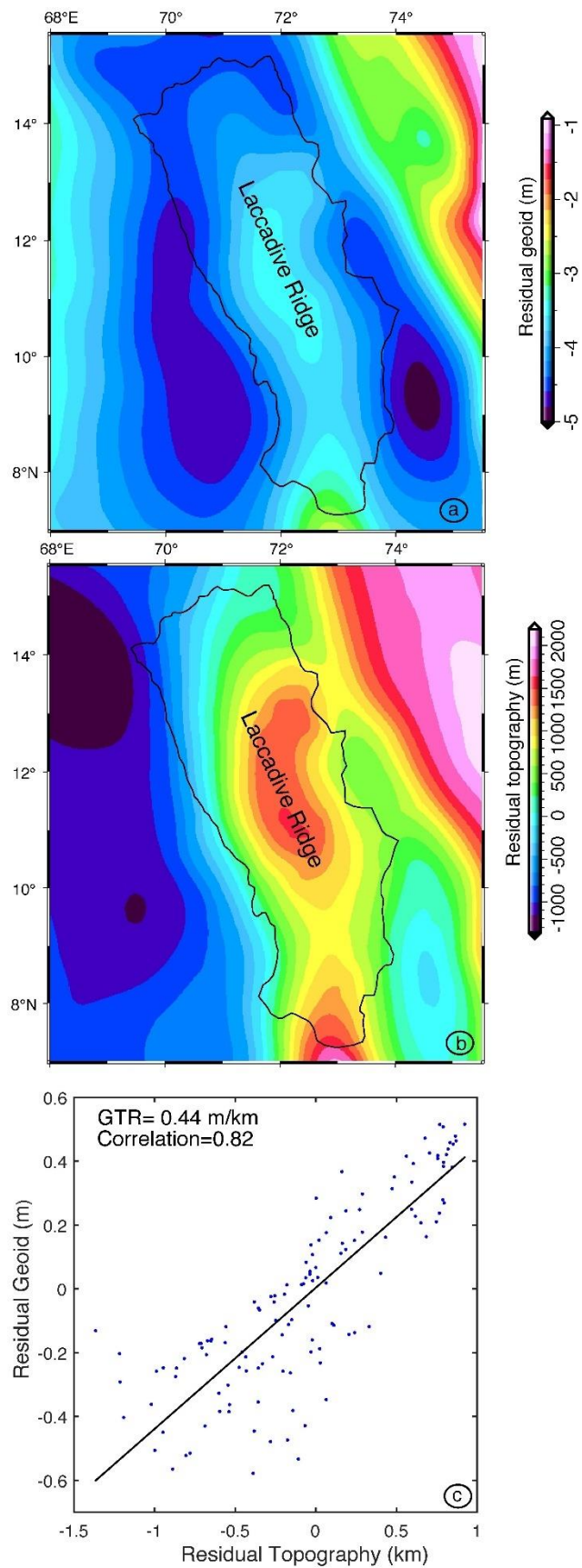


Fig. 6

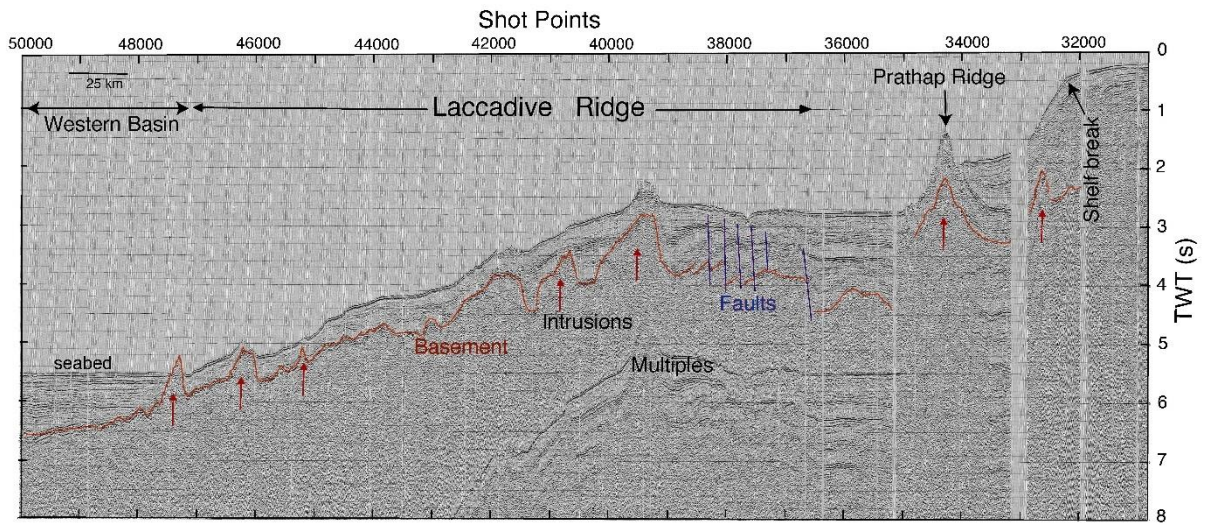


Fig. 7

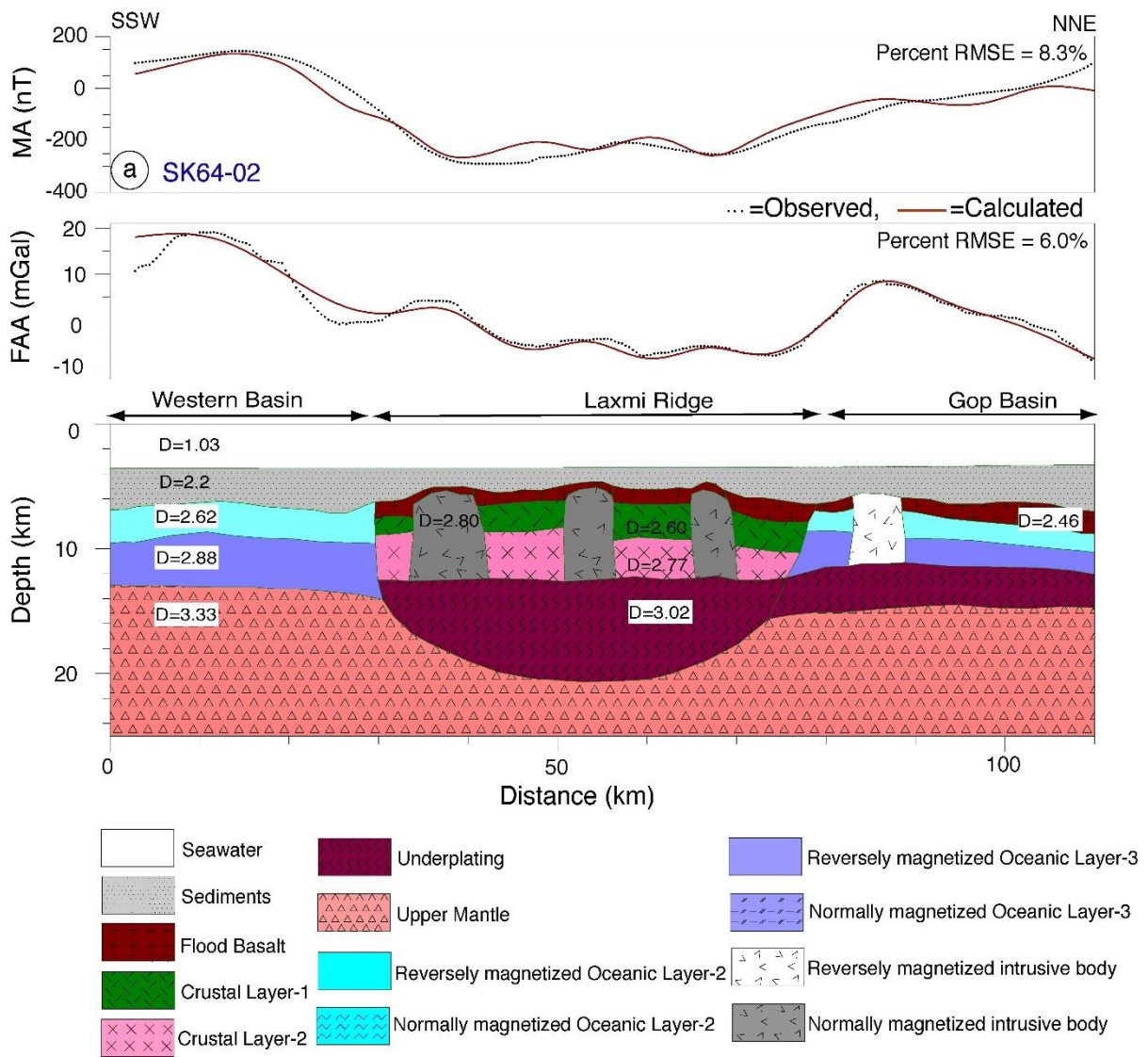


Fig. 8 (a)

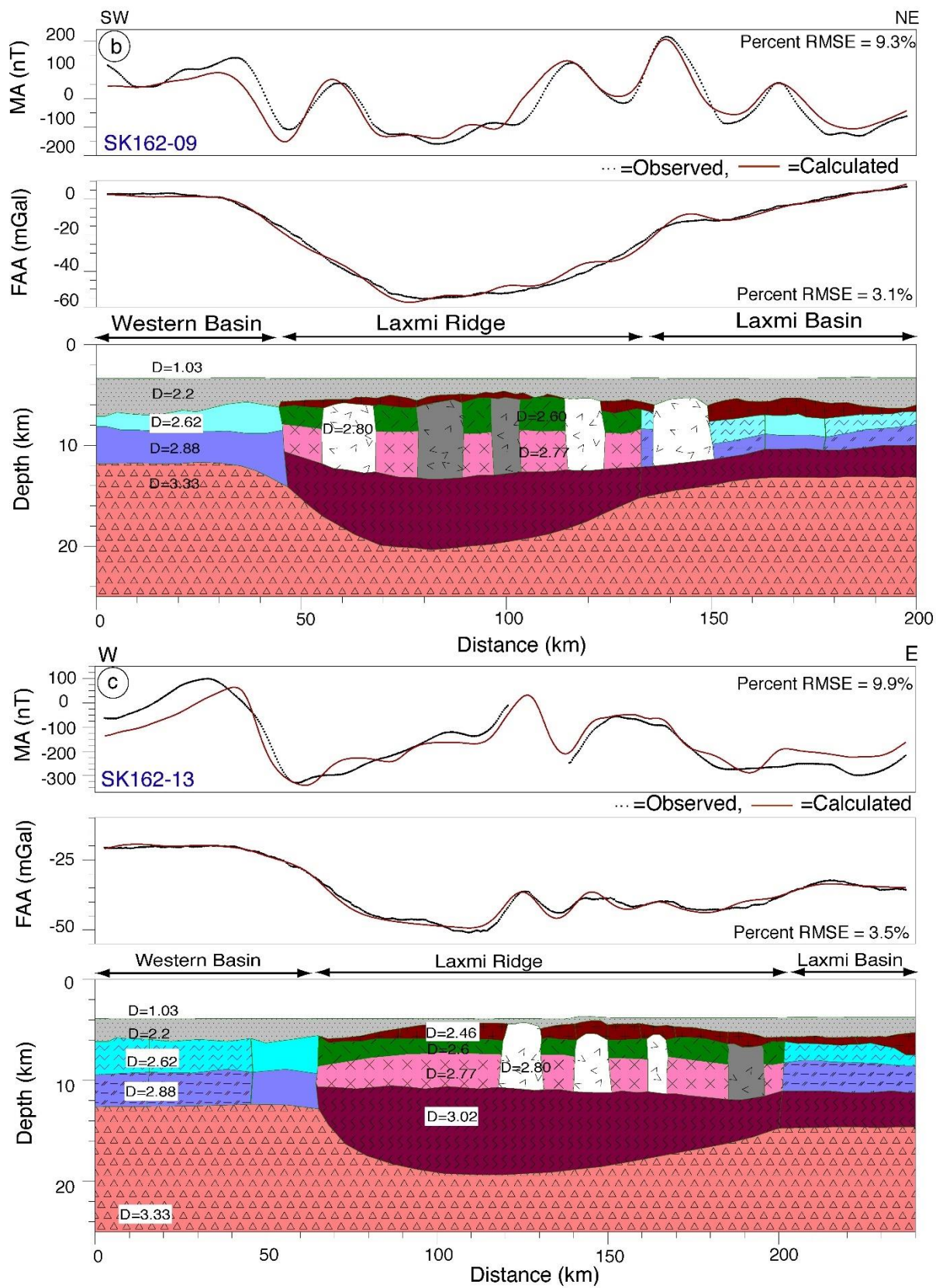


Fig. 8 (b, c)

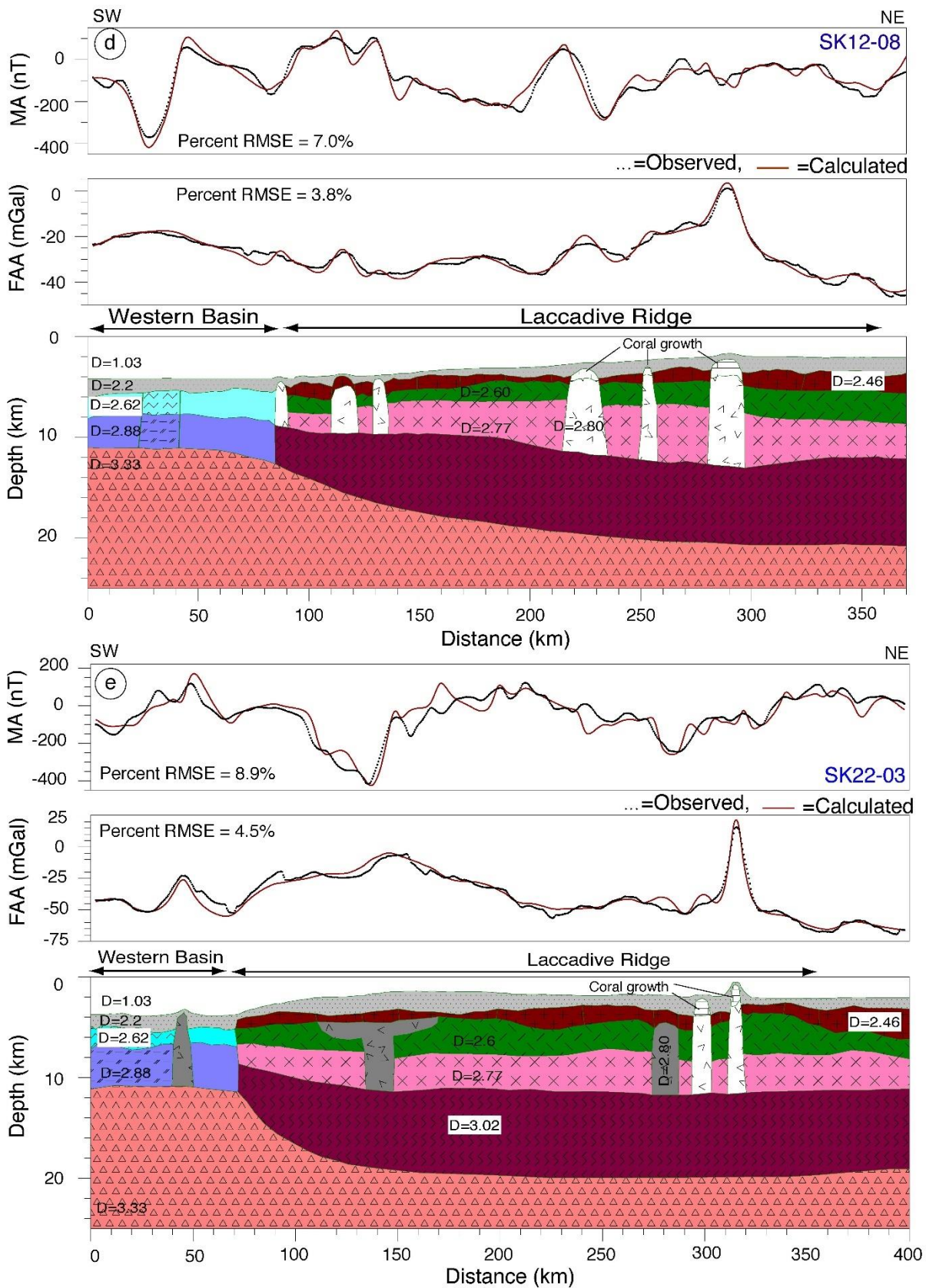


Fig. 8 (d, e)

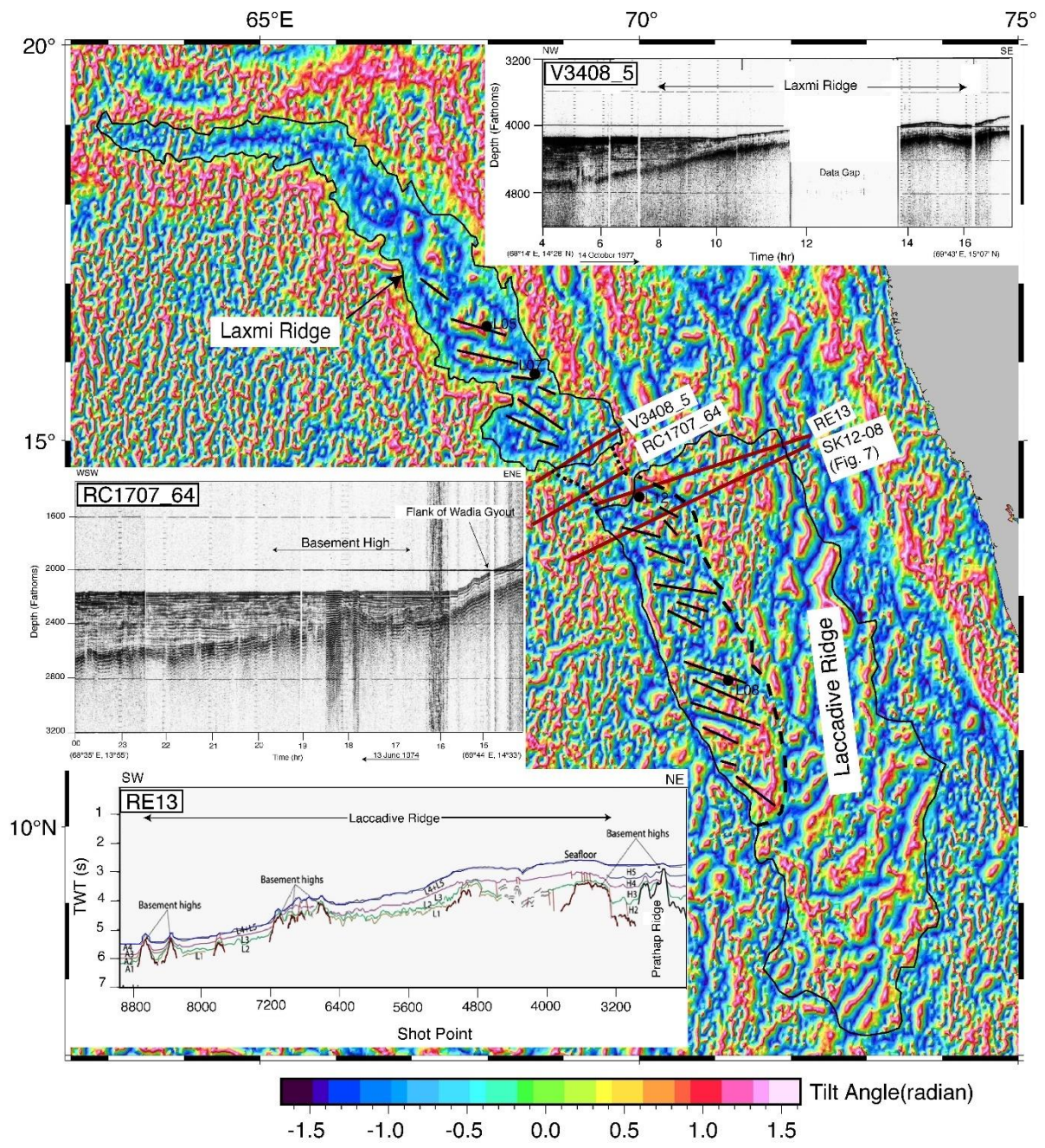


Fig. 9